
End-to-End Differentiable Learning to HDR Image Synthesis for Multi-exposure Images

Jung Hee Kim *

Department of Electronic Engineering
Sogang University
kjhe129@sogang.ac.kr

Siyeong Lee *

NAVER LABS
siyeong.lee@naverlabs.com

Soyeon Jo

Department of Electronic Engineering
Sogang University
soyeonjo@sogang.ac.kr

Suk-Ju Kang

Department of Electronic Engineering
Sogang University
sjkang@sogang.ac.kr

Abstract

Recent deep learning-based methods have reconstructed a high dynamic range (HDR) image from a single low dynamic range (LDR) image by focusing on the exposure transfer task to reconstruct the multi-exposure stack. However, these methods often fail to fuse the multi-exposure stack into a perceptually pleasant HDR image as the local inversion artifacts are formed in the HDR imaging (HDRI) process. The artifacts arise from the impossibility of learning the whole HDRI process due to its non-differentiable structure of the camera response recovery. Therefore, we tackle the major challenge in stack reconstruction-based methods by proposing a novel framework with the fully differentiable HDRI process. Our framework enables a neural network to train the HDR image generation based on the end-to-end structure. Hence, a deep neural network can train the precise correlations between multi-exposure images in the HDRI process using our differentiable HDR synthesis layer. In addition, our network uses the image decomposition and the recursive process to facilitate the exposure transfer task and to adaptively respond to recursion frequency. The experimental results show that the proposed network outperforms the state-of-the-art quantitative and qualitative results in terms of both the exposure transfer tasks and the whole HDRI process.

1 Introduction

Recently, most cameras use the high dynamic range imaging (HDRI) technique because it provides better aesthetic appreciation than ordinary imaging techniques with a limited dynamic range [24]. Moreover, HDRI aims to restore under-exposed and over-exposed regions, so that the reconstructed high dynamic range (HDR) images convey much information such as image details irrespective of the illuminance change. Especially, recent vision systems have used HDRI to improve their performance in terms of robustness and consistency. This is because images captured with conventional cameras can cause the performance degradation of vision systems when the severe luminance variation occurs (e.g., passing through the tunnel). In this context, various approaches such as fusing the multi-exposure stack [4] and implementing the event cameras [28] have been introduced.

Deep neural networks, especially convolutional neural networks (CNNs), have shown their significant role in reconstructing the HDR image. Two primary approaches exist in reconstructing the HDR

*equal contribution

image: direct reconstruction methods [5, 15, 17] and multi-exposure stack-based synthesis methods [6, 13, 14]. Direct reconstruction aims to recover a HDR image (32bits/pixel) from a given single low dynamic range (LDR) image (8bits/pixel). In this case, a large number of LDR-HDR image pair data is required to train a deep neural network [17]. There have been many attempts to solve the data quantity problem by crawling image pairs from the internet or generating synthetic image pairs [15]. On the other hand, HDR synthesis with the multi-exposure stack focuses on transferring exposures to accurately generate the multi-exposure stack. These approaches alleviate the dataset quantity problem [14]; however, they suffer from the severe local inversion artifacts. Furthermore, fusing several up/down exposure images is a non-differentiable process due to the recovery of camera response functions (CRF) [4], with the function having the discrete form. Due to the limitation, the conventional networks cannot be trained in an end-to-end manner reflecting the whole HDRI process.

To alleviate the above problems, we propose the differentiable HDR synthesis process. We also incorporate the image decomposition approach to disentangle an exposure transfer task and the recurrent network to recursively process the sequentially generated images. Our contributions are three-fold as follows:

- We propose a novel framework with a differentiable HDRI synthesis method. To overcome the conventional limitations of multi-exposure stack-based HDR synthesis, We modify the discrete CRF function, which converts pixel intensity values into luminance values in the standard HDRI, to be differentiable with the linear approximation technique.
- We incorporate the image decomposition method for reconstructing the HDR image to focus on preserving the image details in exposure transfer tasks. We disentangle exposure transfer tasks with the two-pathway approach, which adjusts global tone and reconstructs the local structure of the image individually.
- We propose a recurrent approach in the multi-exposure stack generation to efficiently utilize the recursive process. Our network learns to generate sequential images with multiple exposures in the recurrent structure as the recursive process requires to maintain gradients until the entire multi-exposure stack is generated.

2 Related Work

2.1 High dynamic range imaging

Camera response function (CRF) represents the luminance-to-intensity mapping function of the individual camera, which enables to remap the scene luminance from captured images. Debevec and Malik [4] proposed the HDRI pipeline that estimates the CRF from LDR images with different exposures. Estimating the CRF or inverse CRF is modeled as the least-square problem:

$$O = \sum_i^N \sum_j^P [g(Z_{ij}) - \ln E_i + EV_j]^2 + \lambda \sum_{z=Z_{min}+1}^{Z_{max}-1} g''(z)^2, \quad (1)$$

where O denotes an objective function, g denotes an inverse CRF, and Z_{ij} as a pixel intensity value of i -th pixel of j -th exposure value images. Z_{min} and Z_{max} indicates minimum and maximum intensity values of given LDR images. N and P are the number of images and exposure values of the stack, and i , and j are their corresponding indices, respectively. E_i denotes the luminance value of i -th pixel and EV_j denotes the j -th exposure value. The exposure value can substitute exposure time with a fixed aperture and ISO value. The second term of the objective function regularizes the CRF to be smoothened with the hyperparameter λ . By minimizing the objective function, we can obtain the discrete CRF of g , which maps 8-bit pixel intensity values to 32-bit luminance values. Many other approaches to estimate the CRF have been proposed. Robertson *et al.*[22] proposed to apply the Gauss-Seidel method [31] to estimate the CRF and Grossberg and Nayar [8] proposed to jointly estimate intensity mapping functions and exposure ratios to recover the CRF. However, approaches with a multi-exposure image stack suffer the limitation of dataset composition when the perspective alignment of images is required with the entire multi-exposure stack. To overcome the limitation, Bogoni [2] and Kang *et al.*[10] incorporated optical flow-based methods to compensate artifacts, and Kronanader [9] proposed to utilize optical architectures with multiple sensors. However, these methods demand to meet requirements to priory composite images with diverse exposure values.

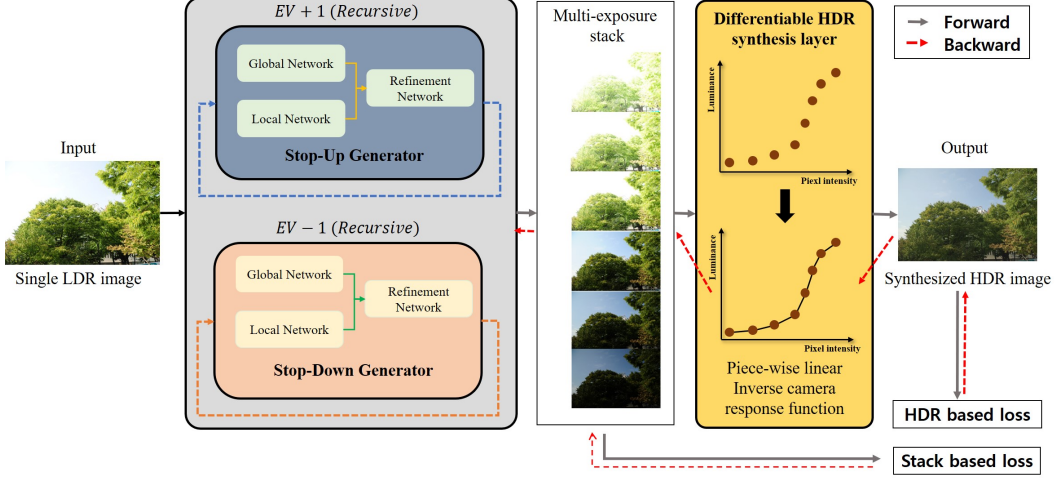


Figure 1: The overall structure of the proposed framework. Our model consists of stop-up and stop-down networks with the differentiable HDR synthesis layer. Given an input LDR image, the multi-exposure image stack is generated with recursions. Then, the generated stack is synthesized to reconstruct the HDR image with the estimated camera response function using Eq. (1).

Moreover, since CRF is a discrete function and non-differentiable, the deep neural network can be partially utilized in the whole HDRI process.

2.2 Deep learning-based HDR reconstruction

Direct HDR reconstruction. The recent development of deep neural networks has imposed on learning the direct mapping function between a single LDR image and a target HDR image. Direct methods generate the HDR image without fusing the image stack of different exposures, thereby removing the ghosting artifacts because spatially aligned multi-exposure image stack is not required. Eilerstsen *et al.*[5] focused on restoring saturated regions of the underexposed LDR image to recover the luminance map, which is combined with the input LDR image to reconstruct the HDR image. Marnerides *et al.*[17] proposed a CNN model that trains to infer a direct mapping function between LDR and HDR images. To overcome the dataset quantity challenges, Kim *et al.*[12] and Liu *et al.*[15] utilized the dynamic range constrained dataset, which consists of images crawled and extracted from the Internet, and the virtual dataset, respectively. However, since the datasets have diverse dynamic ranges, the normalization or standardization process for the images becomes difficult. Due to the undetermined dynamic range of images, the models might be trained in the wrong direction, on the account of the gap between virtually generated images and real images.

Multi-exposure stack HDR synthesis Multi-exposure stack HDR synthesis methods incorporated the deep neural network to generate multi-exposure image stack. The ambiguity of the LDR-to-HDR mapping relation is avoided by focusing on the intermediate task of generating multi-exposure stack. Endo *et al.*[6] and Lee *et al.*[13, 14] focus on reconstructing the multi-exposure stack from a single LDR image to synthesize a target HDR image. However, these approaches cannot learn the entire HDRI process because CRF is not differentiable, thereby generating severe local inversion artifacts on reconstructed images [14].

3 End-to-end Differentiable Learning to HDR Image Synthesis

This section describes our end-to-end differentiable learning framework that trains both the exposure transfer process for multi-exposure stack generation and the HDR image synthesis, as shown in Fig. 1. We first generate the multi-exposure stack with the recursive process for stop-up and stop-down networks to reconstruct the entire stack. We then synthesize the stack with the differentiable HDR synthesis layer to reconstruct the HDR image, and train the network in end-to-end structure. In addition, we describe our recurrent network that restores details in saturated regions of the multi-exposure stack, by incorporating the image decomposition approach.

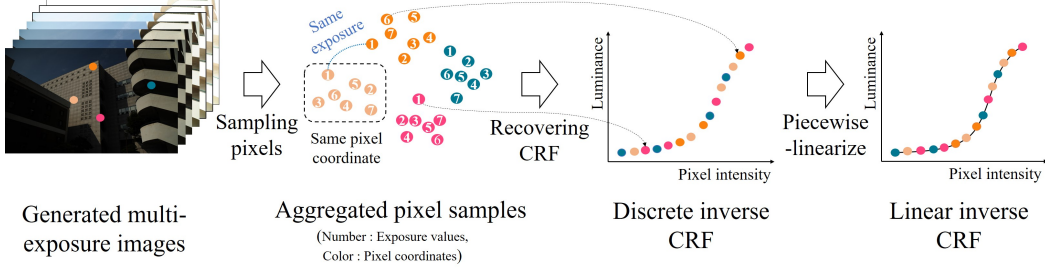


Figure 2: Conceptual diagram of the proposed piece-wise linearization for the CRF. We sample pixels from the multi-exposure stack to aggregate pixels of same coordinate with different exposure values. We then estimate the inverse CRF with Eq. (1) and convert the function into a linear form with the piece-wise linearization.

3.1 Differentiable HDR synthesis layer

The inverse CRF g is estimated by minimizing the objective function of Eq. (1), which can be derived from the multi-exposure stack. Typically, the inverse CRF is a non-differentiable mapping function with discrete values, thereby non-trainable in the deep neural network. The estimated inverse CRF remaps the pixel intensity value to the luminance value as follows.

$$\ln E_i = g(Z_{ij}) - EV_j, \quad (2)$$

where Z_{ij} is the i -th pixel intensity value of j -th exposure image and E_i is the luminance value of a given pixel Z_{ij} . EV_j denotes the j -th exposure value. The scene luminance is remapped with Eq. (2); however, it has the form of the non-differentiable function. We transform the inverse CRF with a linear approximation technique.

Let an inverse CRF be $g = [p_0, p_1, \dots, p_N]$ with N denoting the maximum intensity value of multi-exposure images. We define the derivative of the linearized function \hat{g} as follows.

$$\frac{\partial \hat{g}}{\partial Z_{ij}} = \begin{cases} g(0), & \text{if } Z_{ij} = 0 \\ g(Z_{ij}) - g(Z_{ij} - 1), & \text{otherwise.} \end{cases} \quad (3)$$

Fig. 2 illustrates our approach to piecewise-linearize the inverse CRF. The linearization method is applied with the prior assumptions of the CRF having the characteristic of monotonically increasing with the shape of the smooth curve. We reformulate the function with a piece-wise linear form to back-propagate the difference between the function value and the one before as shown in Eq. (3). The simple linearization method enables the propagation of gradients to each pixel of the multi-exposure stack with the chain rule [7]. The gradients from the loss of luminance values flow to pixel intensity values of each image, which imposes constraints on the generated multi-exposure stack to have correlated values with Eq. (3). Hence, the differentiable HDR layer exploits the network to learn both the multi-exposure stack generation task and the HDR synthesis task. We tested our differentiable HDR layer output to reproduce the identical results with the MATLAB HDR Toolbox [1] and to generate a pixel-wise gradient.

3.2 Recursive multi-exposure stack generation

We incorporate the recursive generation of the multi-exposure image stack with the prior knowledge of the exposure manifold space [14]. We propose the stop-up and stop-down networks to be distinct from conventional methods [13, 14]. Since the process is defined as a recursive process, we implement the convolutional gated recurrent unit (Conv-GRU) [25] to construct the recurrent network. In addition, as multi-exposure images have different over-exposed and under-exposed regions regarding their exposure values, we decompose the exposure transfer task into two path-ways. From a given single image, our model learns the global tone and local details individually. Furthermore, the refinement network integrates global and local components to generate fine-tuned images.

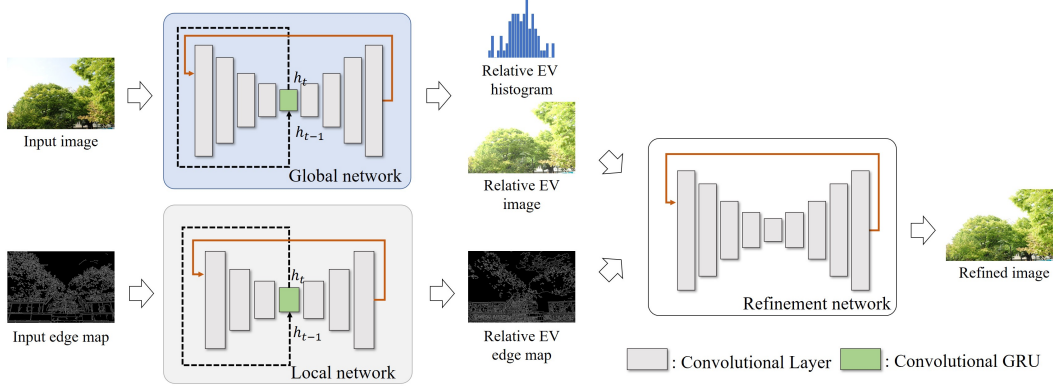


Figure 3: Sub-networks architecture. The global network matches the histograms of relative EV images and the local network focuses on generating gradient-based edge structures. We then concatenate the input image, relative EV image, and edge map to feed into the refinement network. We facilitate the hidden state h_t of t -th recursion to feed into the bottleneck layer.

Fig. 3 shows the structures of sub-networks in our model. Our stop-up and stop-down networks contain three sub-networks of U-Net structures [23] to transfer exposures to the images with the relative up and down EVs: the global, local, and refinement networks. The global and local networks are constructed with 5-level and 4-level structures, respectively, with 2 convolutional layers for each level. We implemented the Swish activation [20] on each convolution layer to alleviate a gradient vanishing problem. Note that the refinement network shares the same structure with the global network except for the Conv-GRUs on bottleneck layers. We impose the global and local networks to adaptively respond the number of recursions and the refinement network to focus on combining the global and local components, which are global tones and gradient-based edge structures of a target LDR image, respectively. Moreover, the refinement network is trained to improve the perceptual quality of the generated image.

The stop-up (or stop-down) network exploits the same weights for transferring exposures, even with the recurrent state that differs from the exposure value of an input. However, both the stop-up and stop-down networks should adaptively produce the over-exposed and under-exposed images corresponding to the exposure value of an input. Therefore, we use the conditional instance normalization to standardize feature maps of different exposure values. The normalization transforms a feature map, X , of which the shape is $C \times H \times W$, into a normalized map Y by using two learnable parameters of γ_e and β_e with the target exposure value of e , which are in \mathbb{R}^C . The normalized map is formulated as $Y = \frac{\gamma_e(X - \mu) + \beta_e}{\sigma}$, where μ and σ are the mean and the standard deviation of X taken across spatial axes, respectively. In other words, our networks select the scale and shift factors according to the exposure value of an input LDR image. By using the conditional instance normalization, we can assist the network to focus on detecting subtle differences between the estimated and target images. Thus, we implemented a conditional instance normalization layer on the decoding layers of each level.

Training The stop-up and stop-down networks are trained separately with a given single LDR image to recursively generate the multi-exposure stack. For the sub-networks, the global and local networks are trained individually in advance, then we jointly trained the entire network including the refinement network. The loss functions are defined independently with each sub-network. Specifically, the global network is trained with the pixel-wise L_1 loss (L_1) and histogram loss (L_{hist}) to constraint the network to generate the image with similar global tone to the target image. The local network is trained with pixel-wise L_1 loss (L_{edge}) on edge maps computed with Canny edge detector [3] of $\sigma = 2$. The refinement network is trained with L_1 loss (L_1), the contextual bilateral loss (L_{CoBi}) [32], and the HDR loss (L_{HDR}). For the HDR loss, we used a tone-mapped HDR loss with μ -law to stabilize the training process [29]. Note that L_{CoBi} alleviates the ghosting artifacts due to the misaligned images by minimizing the distances between the matching features extracted from the 3-rd and 4-th layer of the pre-trained VGG-19 network [26] with the bilateral filtering. Overall loss functions are formulated as follows:

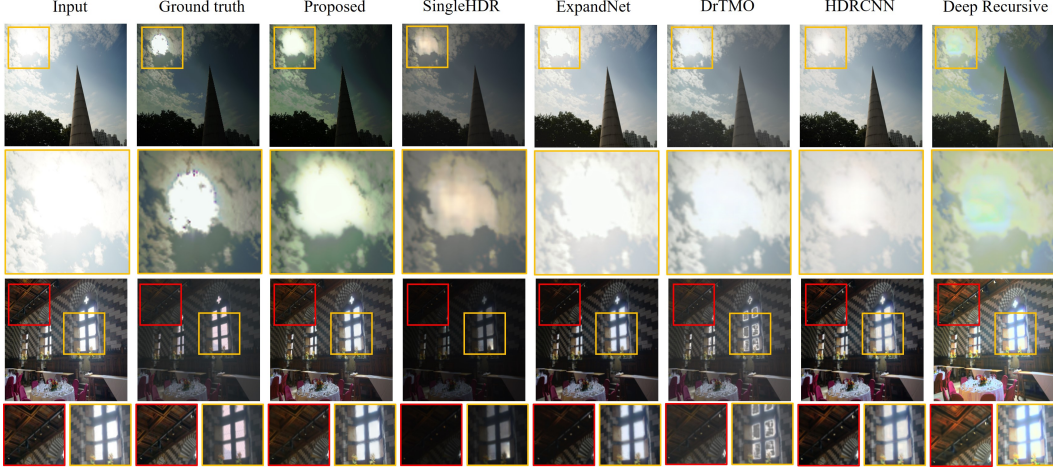


Figure 4: Comparison of tone-mapped HDR images from 6 different HDR reconstruction approaches on VDS and HDR-Eye datasets [19]. The loss of image details in over-exposed and under-exposed regions occurs with the SingleHDR [15], ExpandNet [17], and HDRCNN [5]. The DrTMO [6] and Deep recursive HDR [14], which are stack-based methods, suffer from the local inversion artifacts. Nonetheless, our method reduces local inversion artifacts and preserves image details and contrasts in overexposed regions.

$$L_{global} = \lambda_1 L_1 + \lambda_2 L_{hist} = \frac{\lambda_1}{N \cdot E} \sum_e \sum_i |\hat{I}_i^e - I_i^e| + \frac{\lambda_2}{L \cdot E} \sum_e \sum_l |cnt_l(\hat{I}^e) - cnt_l(I^e)| \quad (4)$$

$$L_{local} = \lambda_3 L_{edge} = \frac{\lambda_3}{N \cdot E} \sum_e \sum_i |\hat{E}_i^e - edge(I_i^e)| \quad (5)$$

$$L_{refine} = \lambda_4 L_1 + \lambda_5 L_{HDR} + \lambda_6 L_{CoBi} \quad (6)$$

$$= \frac{\lambda_4}{N \cdot E} \sum_e \sum_i |\hat{I}_i^e - I_i^e| + \frac{\lambda_5}{N} \sum_i \left| \log \frac{1 + \mu \hat{H}_i}{1 + \mu H_i} \right| + \frac{\lambda_6}{M} \sum_j \min_k (\mathbb{D}_{p_j, q_k} + w_s \mathbb{D}'_{p_j, q_k}) \quad (7)$$

where N , E , L , and M denote the number of pixels, exposure values, intensity levels, and features respectively, and for all the equations, $\hat{\cdot}$ represents the prediction of the network. I_i^e denotes the i -th pixel value in image I of exposure value e , and $cnt_l(\cdot)$ indicates the number of pixels which has a rounded down intensity l in the input image I . $edge(\cdot)$ extracts gradient-based edge maps from the image I , and E_i denotes the i -th pixel value in predicted edge map. H_i is a pixel luminance in the HDR image, and μ is the compression parameter of the HDR image, where we set the value with 5000. $\mathbb{D}_{i,j}$ indicates the sum of cosine distances between all the matched features of p and q , and $\mathbb{D}'_{p,q}$ indicates spatial coordinate distance. Note that j and k indicate indices of the matched feature of p and q respectively. We set the hyperparameters $\lambda_1 = \lambda_3 = \lambda_4 = \lambda_5 = 1$ and $\lambda_2 = \lambda_6 = 0.1$ in our experiments.

4 Experimental Results

4.1 Experiments setups

Datasets We trained our model on the VDS dataset [13], where the training set has 48 multi-exposure stacks and the testing set has 48 stacks. In addition, we evaluated our model on the stacks of HDR-Eye dataset [13, 15, 19], which is widely used for the performance evaluation. Input images were upscaled or downscaled into 256×256 pixel resolutions by the Lanczos interpolation method [11], and all LDR images are in the sRGB color space.

Table 1: Quantitative comparison of proposed and conventional HDR reconstruction methods. We measured HDR-VDP-2 score [16] for synthesized HDR images.

Method	VDS		HDR-Eye	
	m	σ	m	σ
Proposed	63.481	4.401	61.545	2.787
HDRCNN [5]	45.851	7.087	48.629	1.278
DrTMO [6]	51.162	3.845	51.416	6.576
Deep recursive HDRI [14]	58.193	4.792	54.355	4.072
ExpandNet [17]	52.028	4.001	58.887	2.761
SingleHDR [15]	53.462	3.866	59.681	4.352

Table 2: Quantitative comparison of stack reconstruction results. Relative EV+1 indicates the average value of three recursive stop-up results and Relative EV-1 indicates the average value of three stop-down results.

Method	PSNR		SSIM		MS-SSIM	
	m	σ	m	σ	m	σ
Relative Proposed	30.292	3.725	0.952	0.050	0.989	0.009
EV +1 Deep recursive HDRI[14]	30.142	2.873	0.955	0.036	0.986	0.010
Relative Proposed	30.403	3.601	0.940	0.038	0.985	0.011
EV -1 Deep recursive HDRI[14]	30.483	3.836	0.936	0.044	0.982	0.014

Implementation For training the stop-up and stop-down networks, we chose the gradient centralized Adam optimizer [30] with the learning rate of $1e^{-4}$. The momentum parameters of β_1 and β_2 were set to 0.5 and 0.999, respectively. We trained our model with the batch size of 1. In addition, we trained our model on two GTX Titan X GPUs for three days to reach 70k iterations.

Evaluation metrics Our model was evaluated with the HDR-VDP-2 score [15–17] for HDR reconstruction results. We preprocessed reference HDR images with the range normalization [17] before measuring the HDR-VDP-2 score, which is set to a viewing distance of 0.5 m, the color encoding of RGB-BT.709 for a 24-inch display. We also assessed the quality of estimated multi-exposure stacks with peak signal-to-noise ratios (PSNR), structure similarity (SSIM), and multi-scale SSIM (MS-SSIM). We then used the method of Reinhard *et al.*[21] for visualization.

4.2 Comparison with the state-of-the-art methods

HDR reconstruction Our method was compared with both direct methods and multi-exposure stack-based methods as benchmarks. As multi-exposure stack-based methods required the HDR synthesis, we applied the method of Debevec and Malik [4]. Table 1 presents that our method overcame the limitations of the existing methods as it removes the local inversion artifacts and preserves details in over-exposed regions.

Multi-exposure stack reconstruction We verified the relation between the multi-exposure stack reconstruction and the HDR reconstruction. Specifically, we evaluated PSNR, SSIM, and MS-SSIM results of reconstructed stacks by our method and the previous stack-based method [14]. The conventional approach [14] focused on reconstructing the multi-exposure stack, and hence, reproducing stacks with high PSNRs, SSIMs, and MS-SSIMs. However, with the results of Fig. 5 and Table 2, our method reproduced similar PSNR, SSIM, and MS-SSIM with the previous method, but achieved much higher HDR-VDP-2 scores. With the results, we verified that the multi-exposure stack reconstruction and the final HDR reconstruction might not have the precise correlations and that our differentiable HDR synthesis layer imposed a constraint on the network to generate the target HDR image with the highest quality, thereby providing higher HDR-VDP-2 scores.

4.3 Ablation studies

We evaluated the effectiveness of the individual components in our model on the VDS dataset, as shown in Table 3. We added modules incrementally on the U-Net structure[23], which is a baseline of our model with 5-level and 2 convolutional layers for each level, and evaluated with the HDR-VDP-2

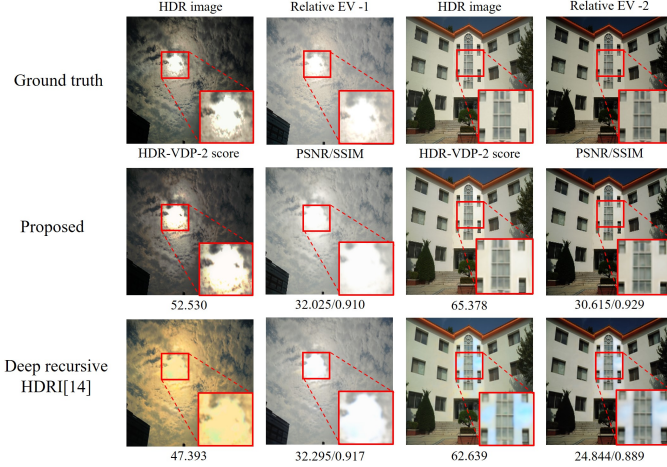


Figure 5: Case analysis of correlations between the multi-exposure stack reconstruction and the HDR reconstruction on the VDS dataset. The experiment was conducted with Lee *et al.* [14] and our proposed method. The result shows that two factors (stack reconstruction accuracy, HDR reconstruction accuracy) have the weak correlation.

Table 3: Performance of various configurations on the VDS dataset [13]

Method	HDR-VDP-2	PSNR (dB)	SSIM
Baseline	53.436 \pm 5.300	25.864 \pm 3.013	0.909 \pm 0.051
+ Recurrent network	56.505 \pm 5.572	27.652 \pm 3.189	0.927 \pm 0.043
+ Conditional instance normalization	57.235 \pm 5.110	27.996 \pm 2.779	0.924 \pm 0.052
+ Image decomposition	58.884 \pm 6.627	28.542 \pm 3.500	0.926 \pm 0.054
+ Differentiable HDR synthesis layer	62.408 \pm 4.053	29.592 \pm 3.596	0.933 \pm 0.052
+ Contextual bilateral loss	63.481 \pm 4.401	30.347 \pm 3.663	0.946 \pm 0.044

score. The overall results show that our method using all modules improved 10.045, 4.483, and 0.037 with HDR-VDP-2 score, PSNR and SSIM, respectively.

Recurrent network First, we added the recurrent module, which is the Conv-GRU [25] to be located in the bottleneck layer. We utilized the hidden state of each recurrent network to convey the import state variables such as recursion numbers to the network. Table 3 shows that recurrent module could increase both the HDR reconstruction performance with HDR-VDP-2 score, and multi-exposure stack reconstruction with PSNR, and SSIM by 3.069, 1.788, and 0.018, respectively.

Conditional instance normalization We demonstrated the effectiveness of the conditional instance normalization layer with comparison experiment with the instance normalization layer [27]. We confirmed that the conditional instance normalization layer decreases the standard deviation of the reconstruction error.

Image decomposition We decomposed input images into global and local components. To verify the effectiveness of our structure, we compared the PSNR result of the decomposition network with that of the baseline network, as shown in Table 3. We trained both networks for the same iterations, and the quantitative results of PSNR and SSIM show that decomposition decreases the reconstruction error.

Differentiable HDR synthesis layer The proposed differentiable HDR synthesis layer could reconstruct the target HDR image without any learnable parameters in the layer. The mean of HDR-VDP-2 score was significantly increased by up to 3.439, and the standard deviation was decreased by up to 2.494. Hence, the differentiable HDR synthesis layer guided the network to generate the high-quality HDR image while stabilizing the training process.

Contextual bilateral loss To enhance the perceptual quality of the generated multi-exposure stack, we added contextual bilateral loss [32] to fine-tune our networks. This loss alleviated the limitations of using ghosting artifacts induced by applying L_1 loss on the misaligned image dataset. Table 3 shows that contextual bilateral loss fine-tunes the outputs of networks.

5 Conclusion

This paper presented a novel framework that learns to generate both the multi-exposure stack and the HDR image. In addition, we proposed a differentiable HDR synthesis layer that converts the HDR synthesis process to be differentiable with the linear approximation technique. Hence, our approach enabled a total network to be trained for the multi-exposure stack generation and the HDR synthesis in an end-to-end manner. Moreover, we adopted recurrent and decomposition approaches that facilitate the multi-exposure stack generation to be more adaptive to input images and to disentangle exposure transfer tasks. The results showed that our framework could get the state-of-the-arts results for both direct and stack-based methods by removing the severe local inversion artifacts and restoring the details regardless of image conditions. For the future work, as we yielded impressive results regarding the relatively low PSNR, we will further analyze the relationship between the multi-exposure stack generation and the HDR image synthesis to optimize multiple tasks to be mutually complementary.

Broader Impact

As we focus on theoretical grounds for restoring the HDR image, it has both positive and negative sides. On the negative side, our method is prone to be exploited like face generation and autonomous system attack [18], even if our method restores lost information based on the context of an input image. However, realistic images can be easily acquired from LDR images taken by a standard camera through our method. Depending on the applications using this method (e.g., autonomous driving, etc.), users should consider foreseeable potential risks, where the contents of the output images may be changed by adversarial attacks for the stop-up or stop-down networks.

References

- [1] Francesco Banterle, Alessandro Artusi, Kurt Debattista, and Alan Chalmers. *Advanced High Dynamic Range Imaging (2nd Edition)*. AK Peters (CRC Press), Natick, MA, USA, July 2017. ISBN 9781498706940.
- [2] Luca Bogoni. Extending dynamic range of monochrome and color images through fusion. In *Proceedings 15th International Conference on Pattern Recognition. ICPR-2000*, volume 3, pages 7–12. IEEE, 2000.
- [3] John Canny. A computational approach to edge detection. *IEEE Transactions on pattern analysis and machine intelligence*, (6):679–698, 1986.
- [4] Paul E Debevec and Jitendra Malik. Recovering high dynamic range radiance maps from photographs. In *ACM SIGGRAPH 2008 classes*, pages 1–10. 2008.
- [5] Gabriel Eilertsen, Joel Kronander, Gyorgy Denes, Rafał K Mantiuk, and Jonas Unger. Hdr image reconstruction from a single exposure using deep cnns. *ACM Transactions on Graphics (TOG)*, 36(6):1–15, 2017.
- [6] Yuki Endo, Yoshihiro Kanamori, and Jun Mitani. Deep reverse tone mapping. *ACM Trans. Graph.*, 36(6):177–1, 2017.
- [7] Ian Goodfellow, Yoshua Bengio, and Aaron Courville. *Deep learning*. MIT press, 2016.
- [8] Michael D Grossberg and Shree K Nayar. Determining the camera response from images: What is knowable? *IEEE Transactions on pattern analysis and machine intelligence*, 25(11):1455–1467, 2003.
- [9] Saghi Hajisharif, Joel Kronander, and Jonas Unger. Adaptive dualiso hdr reconstruction. *EURASIP Journal on Image and Video Processing*, 2015(1):41, 2015.
- [10] Sing Bing Kang, Matthew Uyttendaele, Simon Winder, and Richard Szeliski. System and process for generating high dynamic range video, June 3 2008. US Patent 7,382,931.
- [11] Turkowski Ken. Filters for common resampling tasks, graphics gems i, 1990.
- [12] Soo Ye Kim, Jihyong Oh, and Munchurl Kim. Jsi-gan: Gan-based joint super-resolution and inverse tone-mapping with pixel-wise task-specific filters for uhd hdr video. *arXiv preprint arXiv:1909.04391*, 2019.
- [13] Siyeong Lee, Gwon Hwan An, and Suk-Ju Kang. Deep chain hdri: Reconstructing a high dynamic range image from a single low dynamic range image. *IEEE Access*, 6:49913–49924, 2018.

- [14] Siyeong Lee, Gwon Hwan An, and Suk-Ju Kang. Deep recursive hdri: Inverse tone mapping using generative adversarial networks. In *Proceedings of the European Conference on Computer Vision (ECCV)*, pages 596–611, 2018.
- [15] Yu-Lun Liu, Wei-Sheng Lai, Yu-Sheng Chen, Yi-Lung Kao, Ming-Hsuan Yang, Yung-Yu Chuang, and Jia-Bin Huang. Single-image hdr reconstruction by learning to reverse the camera pipeline. *arXiv preprint arXiv:2004.01179*, 2020.
- [16] Rafat Mantiuk, Kil Joong Kim, Allan G Rempel, and Wolfgang Heidrich. Hdr-vdp-2: A calibrated visual metric for visibility and quality predictions in all luminance conditions. *ACM Transactions on graphics (TOG)*, 30(4):1–14, 2011.
- [17] Demetris Marnerides, Thomas Bashford-Rogers, Jonathan Hatchett, and Kurt Debattista. Expandnet: A deep convolutional neural network for high dynamic range expansion from low dynamic range content. In *Computer Graphics Forum*, volume 37, pages 37–49. Wiley Online Library, 2018.
- [18] Vincent C Müller. Ethics of artificial intelligence and robotics. 2020.
- [19] Hiromi Nemoto, Pavel Korshunov, Philippe Hanhart, and Touradj Ebrahimi. Visual attention in ldr and hdr images. In *9th International Workshop on Video Processing and Quality Metrics for Consumer Electronics (VPQM)*, number CONF, 2015.
- [20] Prajit Ramachandran, Barret Zoph, and Quoc V Le. Searching for activation functions. *arXiv preprint arXiv:1710.05941*, 2017.
- [21] Erik Reinhard, Michael Stark, Peter Shirley, and James Ferwerda. Photographic tone reproduction for digital images. In *Proceedings of the 29th annual conference on Computer graphics and interactive techniques*, pages 267–276, 2002.
- [22] Mark A Robertson, Sean Borman, and Robert L Stevenson. Dynamic range improvement through multiple exposures. In *Proceedings 1999 International Conference on Image Processing (Cat. 99CH36348)*, volume 3, pages 159–163. IEEE, 1999.
- [23] Olaf Ronneberger, Philipp Fischer, and Thomas Brox. U-net: Convolutional networks for biomedical image segmentation. In *International Conference on Medical image computing and computer-assisted intervention*, pages 234–241. Springer, 2015.
- [24] Pradeep Sen and Cecilia Aguerrebere. Practical high dynamic range imaging of everyday scenes: Photographing the world as we see it with our own eyes. *IEEE Signal Processing Magazine*, 33(5):36–44, 2016.
- [25] Mennatullah Siam, Sepehr Valipour, Martin Jagersand, and Nilanjan Ray. Convolutional gated recurrent networks for video segmentation. In *2017 IEEE International Conference on Image Processing (ICIP)*, pages 3090–3094. IEEE, 2017.
- [26] Karen Simonyan and Andrew Zisserman. Very deep convolutional networks for large-scale image recognition. *arXiv preprint arXiv:1409.1556*, 2014.
- [27] Dmitry Ulyanov, Andrea Vedaldi, and Victor Lempitsky. Instance normalization: The missing ingredient for fast stylization. *arXiv preprint arXiv:1607.08022*, 2016.
- [28] Lin Wang, Yo-Sung Ho, Kuk-Jin Yoon, et al. Event-based high dynamic range image and very high frame rate video generation using conditional generative adversarial networks. In *Proceedings of the IEEE Conference on Computer Vision and Pattern Recognition*, pages 10081–10090, 2019.
- [29] Qingsen Yan, Dong Gong, Qinfeng Shi, Anton van den Hengel, Chunhua Shen, Ian Reid, and Yanning Zhang. Attention-guided network for ghost-free high dynamic range imaging. In *Proceedings of the IEEE Conference on Computer Vision and Pattern Recognition*, pages 1751–1760, 2019.
- [30] Hongwei Yong, Jianqiang Huang, Xiansheng Hua, and Lei Zhang. Gradient centralization: A new optimization technique for deep neural networks. *arXiv preprint arXiv:2004.01461*, 2020.
- [31] David M Young. *Iterative solution of large linear systems*. Elsevier, 2014.
- [32] Xuaner Zhang, Qifeng Chen, Ren Ng, and Vladlen Koltun. Zoom to learn, learn to zoom. In *Proceedings of the IEEE Conference on Computer Vision and Pattern Recognition*, pages 3762–3770, 2019.